

3C 254: the alignment effect and unification schemes

M. N. Bremer^{1,2}

¹*Sterrewacht Leiden, Postbus 9513, 2300RA Leiden, Netherlands*

²*Institute of Astronomy, Madingley Road, Cambridge CB3 0HA*

Accepted 1996 August 2. Received 1996 July 11; in original form 1995 August 31

ABSTRACT

3C 254 is a radio-loud quasar at $z=0.734$. Optical line and continuum emission from the underlying galaxy is clearly extended and aligned with the radio axis; the object shows the so-called ‘alignment effect’ which is often seen in powerful radio galaxies. This is the clearest case yet of the continuum alignment effect in a radio-loud quasar. The object is one of the most lobe-dominated 3C quasars; the significance of the aligned emission in this source is discussed in terms of orientation-based unification schemes for radio-loud quasars and radio galaxies. 3C 254 is a very asymmetric radio source and it is shown that the radio structure on the side with the shortest nucleus–hotspot distance is interacting with the emission-line gas surrounding the quasar. It is also shown that the quasar is surrounded by an overdensity of faint objects, consistent with a cluster or group of galaxies around the object.

Key words: galaxies: clusters: general – cooling flows – quasars: emission lines – quasars: individual: 3C 254.

1 INTRODUCTION

3C 254 is a radio-loud quasar (RLQ) at $z=0.734$. Previous work by Forbes et al. (1990, hereafter FCFJ) shows that the quasar is surrounded by line-emitting nebulosity, out to a radius of ~ 80 kpc from the nucleus. The observed [O III]/[O II] line ratio in the extended emission implied that the emitting gas was at high pressure ($> 10^6$ cm⁻³ K within 30 kpc of the nucleus).

The emission-line properties of 3C 254 make it ripe for further investigation. FCFJ argued that the emission-line clouds are pressure confined by a hot medium, cooling at a rate of more than $900 M_{\odot} \text{ yr}^{-1}$ within 35 kpc of the quasar. The cooling medium is most likely to be the intracluster medium (ICM) of a surrounding cluster of galaxies. Any cluster should be detectable in a deep exposure of the quasar field.

Another reason for continued study of 3C 254 is to help determine the connection between powerful (FR II, Fanaroff & Riley 1974) radio galaxies (RGs) and radio-loud quasars (RLQs). Distant powerful RGs often show strong alignment between their radio axes and regions of extended optical continuum and line emission, the so-called ‘alignment effect’ (McCarthy 1993 and references therein). Several authors have suggested that powerful RGs and some (or all) powerful RLQs are drawn from the same parent population, differing in their observed properties because RLQs have their emission axes closer to the line of sight than the RGs (Scheuer 1987; Barthel 1989). Thus,

some quasars should also show the ‘alignment effect’ in both continuum and line emission. The line emission in 3C 254 is the most extended of all of the quasars observed spectroscopically by FCFJ, Bremer et al. (1992), Crawford & Fabian (1989) and Crawford, Fabian & Johnstone (1988). Consequently, it is possible that the extended structure is not as strongly affected by foreshortening and projection effects as other quasars studied in the above work. This makes the quasar a good candidate for examining the connection between RGs and RLQs in terms of their extended optical emission.

The study of the extended emission around 3C 254 can also increase understanding of the various correlations noted between the radio and optical structure of RGs and RLQs. These correlations include the Garrington–Laing effect (Garrington et al. 1988; Laing 1988), the shared radio spectral index/depolarization asymmetry noted by Liu & Pooley (1991), and the emission-line/arm-length asymmetry noted by McCarthy, van Breugel & Kapahi (1991). With these aims in mind, this paper reports further observations of 3C 254 in the ultraviolet (UV), optical and infrared (IR) wavebands.

2 OBSERVATIONS AND RESULTS

2.1 UV spectroscopy

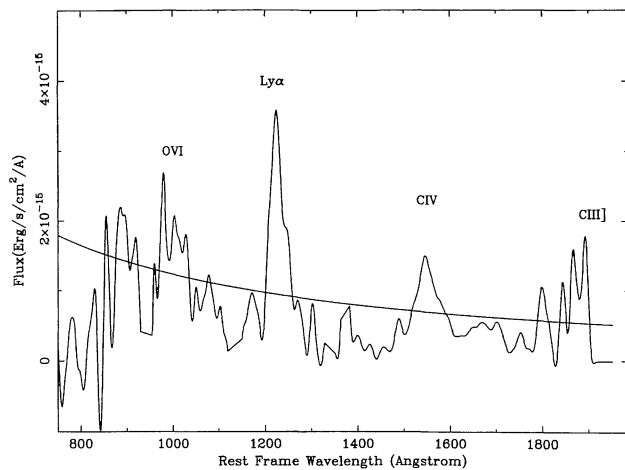
3C 254 was observed by the *International Ultra-violet Explorer (IUE)* using both the SWP and the LWR (see Table 1) in order to better constrain the photoionizing con-

Table 1. Log of observations. (a) Spectroscopy. (b) Imaging.

(a) Telescope	Instrument	Date	Exposure Time (s)	Wavelength Range (Å)	Resolution (Å)	Spatial Resolution (arcsec)
WHT	ISIS (R600R)	1990-Dec-15	3000s	6100-6800	1.5	~ 1
		1991-Jan-15	3000s	8100-8800	1.5	~ 1
IUE	SWP	1992-Feb-19	12300s	1000-2000	5	–
IUE	LWR	1992-Feb-19	7200s	2000-3200	5	–

(b) Telescope	Instrument	Date	Filter	Exposure (sec)	Seeing (arcsec)	Pixel Size (arcsec)	Sensitivity ¹ (Mag.arcsec ⁻²)
WHT	Cass. f/11	1994-Jan-10	<i>U</i>	1200	0.7	0.1	24.0 ± 0.5
		1994-Jan-10	<i>R</i>	600	0.8	0.1	24.0 ± 0.5
WHT	Cass. f/4	1991-May-17	6250/135 ²	500	0.8	0.27	–
		1991-May-17	[O II]/135 ²	900	0.8	0.27	–
CFHT	Cass./Marlin	1992-Jun-20	<i>I</i>	900	1.1	0.36	23.0 ± 0.5
UKIRT	IRCAM	1991-Jan-25	<i>J</i>	900	1.2	0.62	22.5 ± 0.5
		1991-Jan-25	<i>K</i>	900	1.2	0.62	21 ± 0.5

Notes to table:

¹Estimated 3 σ surface brightness limit for object.²Central wavelength/FWHM in Angstrom. [O II] filter centred at 6430 Å.**Figure 1.** *IUE* spectrum of 3C 254. The spectrum is smoothed by a Gaussian of width 100 Å. Systematic noise features have been removed. The over-plotted curve is the best-fit power-law to the ground-based and *HST* spectrum of Wills et al. (1993) normalized to the published magnitudes of the quasar.

tinuum of the quasar and thereby improve the estimate of the pressure of the surrounding environment of the quasar. The spectrum was of poor signal-to-noise ratio. In order to determine the shape of the continuum, it was smoothed with a Gaussian of full width at half-maximum of 100 Å (Fig. 1). The quasar was also observed by the *Hubble Space Telescope* (*HST*) FOS (Wills et al. 1993). This spectrum can be fitted by a power law of slope between $1.3 < \alpha < 1.5$ where $f_{\lambda} = K\lambda^{-\alpha}$ erg cm⁻² s⁻¹ Å⁻¹. Although the true flux scale was not shown by Wills et al., it can be deduced from the published magnitudes of the quasar. This leads to a value of $K = 10^{-10}$ for $\alpha = 1.5$ and $K = 1.7 \times 10^{-11}$ for $\alpha = 1.3$. The latter power law is plotted over the *IUE* spectrum, showing that it is consistent with the UV spectrum. This power law has an energy index of $\alpha_v = 0.7$, where $f_{\nu} \propto \nu^{-\alpha_v}$. The spectrum shows some evidence of a drop-off in the flux

shortward of 900 Å in the rest frame, possibly owing to a Lyman limit system. If so, then the redshift of the absorber is ~ 0.65 . However, given the quality of the spectrum, it is not clear that this feature is real; a further *HST* spectrum is needed. The implications of this result for the estimation of the pressure of the quasar environment are discussed in Section 3.1.

2.2 Optical spectroscopy

3C 254 was observed with the red arm of the ISIS double spectrograph on the William Herschel Telescope (WHT) at a resolution of 1.45 Å (70 km s⁻¹) and a pixel size of 0.7 Å by 0.33 arcsec. Typical seeing was ~ 1 arcsec. Two exposures were made, centred at the wavelengths of redshift [O II] and [O III] (3000 s each). Both exposures were made at position angle 105°, close to the position angle of the radio axis. The slit width was 1 arcsec, comparable to the seeing. Both spectra were taken at low airmass (< 1.2), the effects of differential refraction between the two spectra were minimal.

Figs 2(a) and (b) show a contour plot of the long-slit spectrum around the redshifted [O II] $\lambda 3727$ and [O III] $\lambda 4959, 5007$ emission. They clearly show that the extended emission has a mainly one-sided structure. Both lines show a similar velocity structure, with the high surface brightness extended emission close to the nucleus blueshifted relative to the nuclear line, and the more extended emission at about the same velocity as the nuclear line.

Fig. 3(a) shows the nuclear [O II] and [O III] spectra, extracted from an aperture set slightly above the brightest nuclear row in Fig. 2, to minimize the effects of extended emission in both lines. The extracted spectra were normalized to the total counts in the continuum for each of the two spectra. The [O II] spectrum is offset by 150 counts for display purposes. Clearly nuclear [O III] has a higher equivalent width than nuclear [O II].

Figs 3(b) and (c) show the extended [O II] and [O III] emission extracted from apertures 0.7 to 2 arcsec and 2.3 to

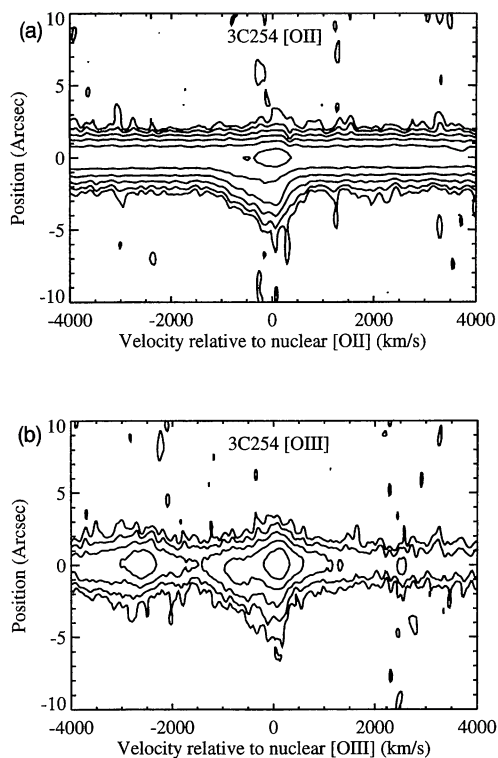


Figure 2. Contour plots of the long-slit spectra of 3C 254 centred at the observed wavelengths of (a) [O II] $\lambda 3727$ and (b) [O III] $\lambda 4959, 5007$. Both lines are extended (out to 5 arcsec in these plots, but to 10 arcsec at lower isophotal levels). Both lines show similar velocity structure; the extended emission close to the nucleus is blueshifted with respect to the nuclear emission. There are subtle differences in the structure, the [O III] emission 650 km s^{-1} shortward of the peak nuclear emission shows an excess at ~ 1 arcsec from the nucleus over the emission from the extended [O II] at a similar velocity shift. This is better shown in Fig. 3. The spectra were taken at a position angle (PA) of 105° . South-east is to the bottom. Contours increase by factors of two in surface brightness. Plots are smoothed in velocity by a $\sim 200 \text{ km s}^{-1}$ FWHM Gaussian.

5 arcsec below (to the south-east of) the peak nuclear row in Fig. 2 respectively. In both cases all seeing-broadened nuclear emission was removed by subtracting off the emission from a spectrum extracted with a similar aperture *above* the nuclear emission. The [O II] spectrum is offset by 35 count for display purposes. The [O III] emission close in to the nucleus is dominated by a component blueshifted by about 650 km s^{-1} relative to the nuclear line. The component is present in the [O II], but it does not dominate to such an extent. Comparing Figs 3(b) and (c) shows that this component represents a small part of the total extended emission-line nebulosity and has a far higher [O III]/[O II] line ratio than the rest of the extended emission in these spectra, or in those of FCFJ. The different ionization and dynamical state of this region probably arises from an interaction between the emission-line clouds and the radio jet of 3C 254 (see later). Approximately 50 per cent of the [O II] emission in the slit comes from off-nuclear regions, whereas only about 20 per cent of the [O III] emission is extended.

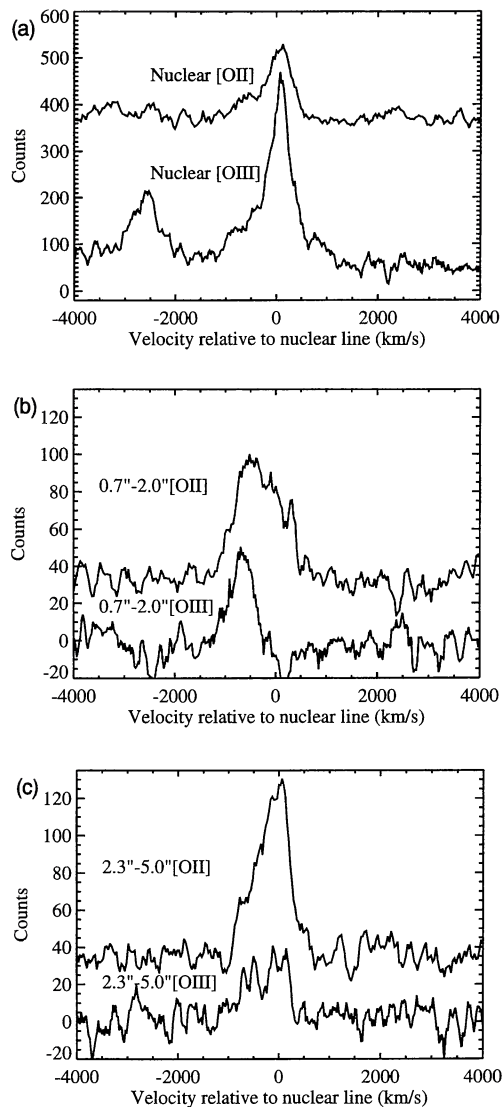


Figure 3. (a) [O II] and [O III] nuclear spectra. To avoid contamination from extended emission lines, the spectra were extracted from just above the peak nuclear rows in Fig. 2. The spectra were then normalized such that the counts in the continuum were the same as those in spectra extracted to include all nuclear emission. The [O II] spectrum is offset by 150 count in order to better display both spectra. (b) [O II] and [O III] spectra extracted from rows 0.7 to 2.0 arcsec to the south-east of the nucleus (i.e. below the nucleus in Fig. 2). Spillover nuclear light was removed by subtracting spectra extracted from the same distance on the other side of the nuclear emission. As these themselves contained a little extended line emission, this caused a slight over-subtraction of line emission at 0 km s^{-1} . Nevertheless, clearly the [O III] emission is dominated by a component blueshifted by $\sim 650 \text{ km s}^{-1}$ relative to the nucleus. The [O II] spectrum is offset by 35 count. (c) As (b) but for the extended emission out to 5 arcsec.

2.3 Optical and IR imaging of the quasar and its field

The log of the optical and IR imaging observations is given in Table 1(b). Photometry of the quasar and the surrounding objects as carried out on each of the continuum frames. For the *U* and *R* frames, GL87 was used for flux calibration (Landolt 1983). For the *I*-band frame, stars in the M92 field (Christian et al. 1985) were used to determine the zero-

point. For the IR frames, GL299 and GL406 were used for calibration. The *URIJK* magnitudes for the quasar are given in Table 2, along with colours for the objects within 10 arcsec of the quasar.

Photometry was carried out using the aperture photometry program *PHOT* in *IRAF*. For the optical images apertures of 1 to 6 arcsec were used to determine the magnitude of 3C 254, to reduce the effect of contamination by the quasar fuzz and nearby objects. In the IR, a constant aperture of 3 arcsec radius was used to stop contamination by nearby companion objects. Determining the colours and magnitudes of the large-scale fuzz was complicated by the lack of a suitable point-spread function (PSF) model for the *U*-band image (there were no bright stars on the frame and the standard star was observed in worse seeing). In each of the *U*, *R* and *I* frames an approximately 1 arcsec² aperture was placed on a region of extended continuum 2 arcsec north-west of the nuclear emission (a region where there is relatively little [O II] emission, see Fig. 5a, in comparison to the continuum emission, see Figs 5b and 4). A similar aperture was placed a similar distance away from the quasar nucleus to the north-east of the nucleus, where there was no extended continuum emission. For each frame, the flux in the second was subtracted from that in the first aperture, thereby removing the influence of the wings of the nuclear PSF; the resultant flux was due to the extended continuum. With the colours of the fuzz known at this spatial position, and assuming that the determined colours were typical of the entire extended continuum, the *U*-band magnitude was determined by scaling the *U*-band surface brightness at the measured position. Given the comparatively poor signal-to-noise ratio of the near IR observations, no determination of the fuzz surface brightness was made in *J* and *K*.

2.3.1 Extended line and continuum emission around 3C 254

All of the optical images show extended emission around 3C 254. The *R*-band image (Fig. 4) is contaminated by [O II] line emission (Fig. 5a), but as shown by the narrow-band (NB) 6250-Å image (Fig. 5b), the continuum is also clearly extended in this band. A comparison of the [O II] and NB images suggest that the line emission is strongest to the east

of the nucleus, and probably dominates the *R*-band emission in the region 1–2 arcsec east of the nucleus in Fig. 4. The slit position used in the spectroscopy cuts through this region. From the estimate of the surface brightness of the extended [O II] emission in FCFJ (2.4×10^{-16} erg cm⁻² s⁻¹ arcsec⁻²), approximately 30–40 per cent of the extended *R*-band light is [O II]. Apart from the emission to the east of the nucleus, the [O II] and NB images are very similar, and so much of the extended structure in the [O II] image may be continuum. However, the spectroscopy of FCFJ clearly shows that there is extended line emission at all position angles around the quasar, although not as strong as the patch 1–2 arcsec east of the nucleus. Most of this emission is not spatially coincident with any radio emission.

Good seeing (0.7 arcsec) and very good pixel sampling (0.1 arcsec pixels) allowed subtraction of 90 per cent of the nuclear light in Fig. 4, using the PSF of a nearby star of similar brightness to the nuclear emission as a model of the nucleus. The resulting image was then smoothed by a Gaussian with FWHM 0.5 arcsec (i.e. slightly smaller than the seeing), to reduce the pixel-to-pixel noise.

The radio map of 3C 254 by Owen & Puschell (1984) is shown as an inset in Fig. 4. The position angle of the current radio axis is approximately 115°. The major axis of the extended line and continuum emission is within about 10° of this, the underlying galaxy shows the same ‘alignment affect’ seen in 3C radio galaxies at the same redshift. The map also shows the very asymmetric nature of the radio structure; the western hotspot and lobe is about 6 times further from the nucleus than the eastern hotspot. The high surface brightness of the emission lines close to the eastern hotspot together with the blueshift seen in the spectra at this position clearly indicate an interaction between the radio structure and emission-line gas at this point.

Many of the high surface brightness features in the extended emission are visible in a lightly smoothed (0.3 arcsec) *HST* image of 3C 254 obtained as part of the *HST* 3C snapshot programme (Lehnert, private communication). For example, the point of emission ~0.8 arcsec south-east of the nucleus is real, it is also present in the [O II], NB and *I*-band images, distorting the lower nuclear isophotes into ellipses in these lower resolution images.

Both the *U*-band (Fig. 5c) and *I*-band (Fig. 5d) images show extended continuum emission aligned along the radio axis. Even though the *U*-band emission is dominated by the very blue nuclear emission, the lower isophotes trace the shape of the extended emission seen in the *R*-band. The *U*-band is uncontaminated by emission lines. The *I*-band includes emission from the extended [O III]. The [O III] and [O II] emission will have the same structure (given the long-slit spectroscopy). Scaling the [O II] surface brightness above by the extended [O III]/[O II] line ratio in FCFJ, the extended [O III] contributes about 20–30 per cent of the extended *I*-band flux. The *I*-band image, like the *R* and *U* images clearly shows several faint objects within 10 arcsec of the quasar.

The optical images show one of the clearest cases of alignment between the extended continuum structure and the radio axis of a radio source at comparatively low redshift. Moreover, the source is a radio-loud quasar rather than a radio galaxy. The [O II] line emission is also clearly aligned. The structure of both extended continuum and line

Table 2. Magnitudes and colours of objects. (a) Magnitudes. (b) Colours.

(a)					
Object	<i>U</i>	<i>R</i>	<i>I</i>	<i>J</i>	<i>K</i>
3C 254	17.4 ± 0.2	17.4 ± 0.2	17.3 ± 0.2	16.5 ± 0.3	15.5 ± 0.3
Quasar Fuzz ¹	20.8 ± 0.3	20.3 ± 0.3	20.0 ± 0.3	–	–
Brightest Companion	< 23.5	22.5 ± 0.2	20.8 ± 0.2	19.5 ± 0.2	18.3 ± 0.3
Other Companions	23.8 ± 0.3	23.1 ± 0.2	21.6 ± 0.2	19.6 ± 0.3	18.6 ± 0.3

(b)			
Object	<i>U</i> – <i>R</i>	<i>R</i> – <i>I</i>	<i>R</i> – <i>K</i>
3C 254	0.0 ± 0.2	0.1 ± 0.3	1.9 ± 0.3
Quasar Fuzz	0.5 ± 0.3	0.3 ± 0.3	–
Brightest Companion	< 0.9	1.7 ± 0.3	4.3 ± 0.4
Other Companions	0.7 ± 0.4	1.5 ± 0.3	4.5 ± 0.4

Notes to table: ¹Magnitudes for fuzz taken by scaling flux in 1 arcsec radius aperture, assuming emission is extended over 15 arcsec².

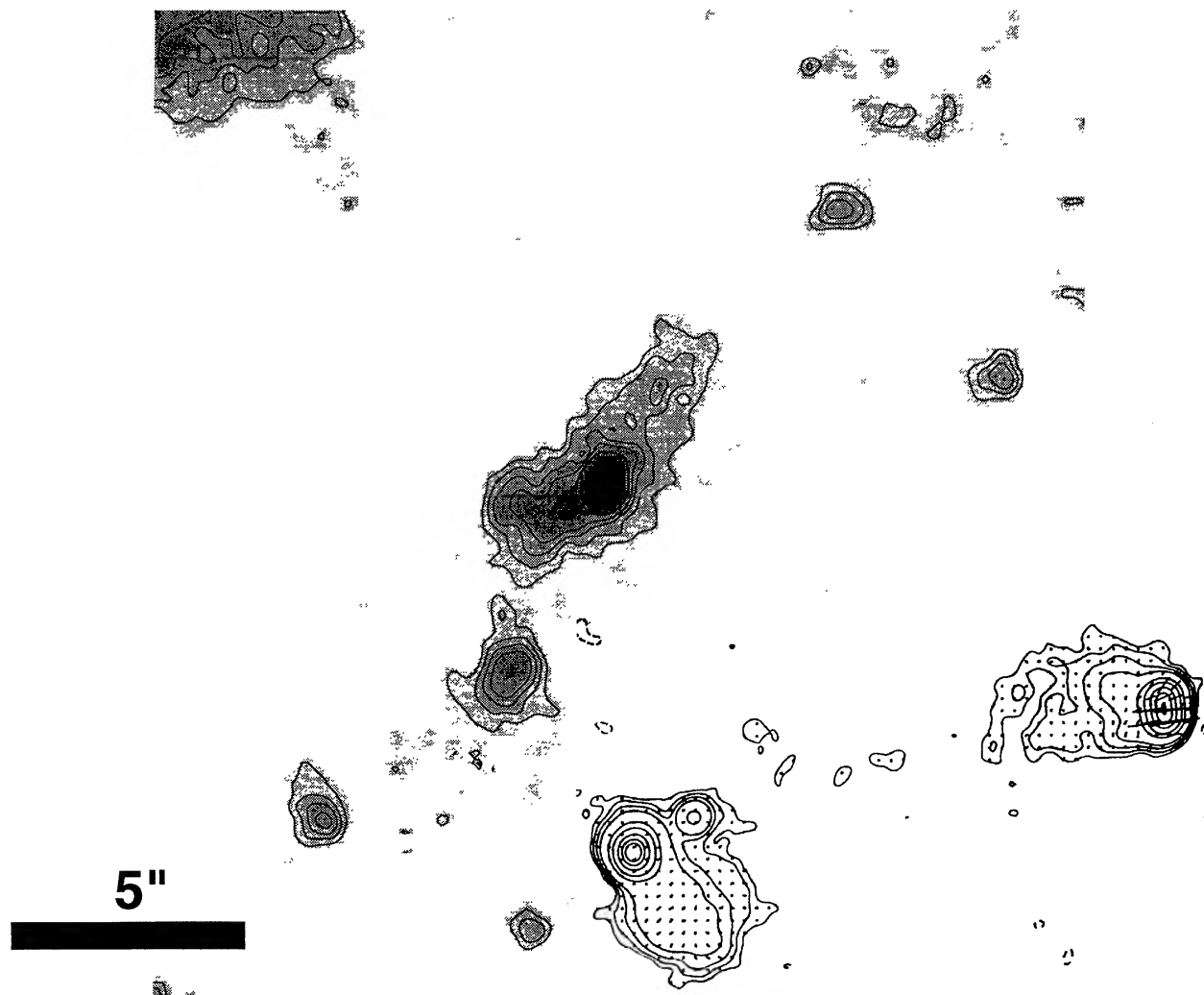


Figure 4. *R*-band image of 3C 254. 90 per cent of the nuclear continuum has been removed by subtracting a scaled PSF made from a nearby star in the frame. The extended emission in this band is both continuum and [O II] line emission. The extended structure aligns with the current radio source axis. Also shown at the same scale, but offset southwards and slightly westwards is the radio map from Owen & Puschell (1984), showing the clearly asymmetric structure of the source. The current radio axis is at a PA of 110° , defined by line through core and eastern hotspot. The western radio arm bends from this PA close to the nucleus, to a more east–west PA at the western hotspot. North is to the top, east is to the left.

emission is comparable to that of similar power RGs at the same redshift.

The *J*- and *K*-band images are noisier than the optical frames due to the stronger emission from the sky in these bands. Nevertheless, the *J*- and *K*-band exposures hint at extended continuum in the lowest isophotal levels with similar continuum structure to that found in the *R*- and *I*-band images.

2.3.2 Clustering of objects around 3C 254

All of the broad-band images show signs of a cluster of faint objects close to the quasar. The section of the *I*-band image in Fig. 5(d) clearly shows four objects within 10 arcsec of the quasar. At least two other fainter objects are also seen in Fig. 5(d) the positions of which correlate with objects seen in other bands. Other fainter objects are in this region, but are not particularly obvious as a result of the isophotal cut

used in Fig. 5(d). These objects are also seen in the *R*-band image. Three of the objects are clearly visible in the *J*-band frame (the restricted field-of-view of IRCAM means that only objects within 8 arcsec of the quasar could be observed). Some of the objects are just visible in the [O II] frame, notably the object 4 arcsec south-east of the quasar, but are fainter in the 6250-Å exposure.

To determine whether the objects around 3C 254 represent a significant overdensity of faint objects, the *I*-band frame was examined by eye and the positions of all objects visible on the frame were noted. This frame was used as it had the largest usable field of view (2 arcmin radius). These positions were used as inputs to an aperture photometry routine written by T. Naylor. This first improved upon the input positions by centroiding within an aperture of 3 arcsec radius. The centroiding was iteratively redetermined until consecutive iterations varied by less than a pixel. The flux within this aperture was then determined and the local sky

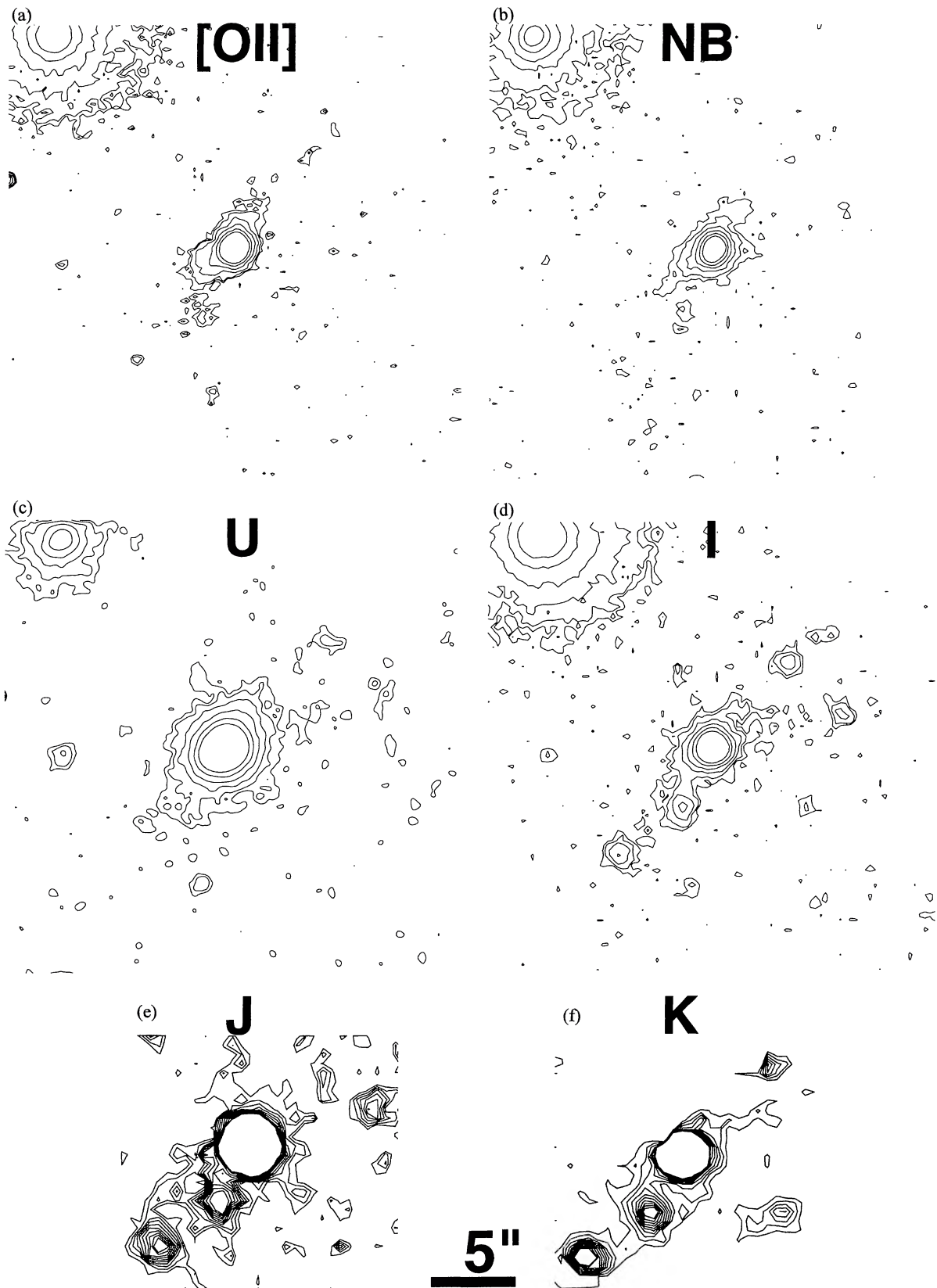


Figure 5. (a) Image in narrow-band filter covering [O II] emission from the quasar. There is some contamination from the continuum, but the [O II] emission extends further to the south-east at PA 115° . This is the emission detected in the long-slit spectrum of [O II] shown in Figs 2(a) and 3(a). (b) Narrow-band continuum image in filter centred at 6250 \AA (FWHM 135 \AA). This image clearly shows the extended continuum emission at a PA of $\sim 115^\circ$. (c) Smoothed *U*-band image of 3C 254. Although nuclear emission is strong in this band, the lower contours clearly show continuum structure similar to that seen in *R* and *I*. (d) *I*-band image of 3C 254. Shows similar extended structure as the *R*-band image. Also clearly shows many relatively faint ($I=21-22$) companion objects. (e) *J*-band and (f) *K*-band images of the immediate environment of 3C 254. Shows companion objects aligned along the radio axis, and lowest contours again suggest extended continuum along the radio axis (although the signal-to-noise ratio is poor). North is to the top, east is to the left.

level subtracted from this flux. The sky level was estimated to be the mode of the pixel values in a box around the object aperture. As has been noted above, there are several objects between 3 and 4.5 mag fainter than the quasar within 10 arcsec. The depth of this exposure meant that these objects are easily visible in the frame. To determine whether this level of clustering was unusual for an object in the field, a subset of objects consisting of all those in the frame between ~ 3 and ~ 5 mag fainter than the quasar ($I=20.4$ and 22.4) was constructed. The upper flux limit was taken to exclude objects too bright to be galaxies at the redshift of the quasar. The lower limit was taken to exclude objects in a range so faint that the sample was incomplete at this level (unresolved objects 5 mag fainter than the quasar are obvious on the frame). Using a lower limit at this level meant that finding the objects by eye was as accurate as an automated source detection program (at least to these levels). Fig. 5(d) shows that the companion objects, and therefore also the sample of all similar magnitude objects on the frame, are clearly detected in the exposure. A plot of surface density of such objects as a function of distance from the quasar (binned into 10 arcsec annuli) is shown in Fig. 6(a). It is immediately obvious that there is a large overdensity of objects (2.2×10^{-2} arcsec $^{-2}$, or seven objects) within 10 arcsec of 3C 254 in comparison to the local field background. All of the other bins are consistent with a faint object density of 3×10^{-3} arcsec $^{-2}$, similar to the background level of objects in the I -band frame of 3C 263 found by Crawford et al. (1991).

To determine the clustering properties on 10 arcsec scales of the other faint sources in the I -band, the number of faint sources within 10 arcsec of each object in the above subsample was determined. Fig. 6(b) shows a histogram of the number of objects with a given number of neighbours within 10 arcsec, for objects in the faint subsample. Also included was 3C 254 itself. This clearly shows that 3C 254, with seven nearby objects in the sample, has unusual clustering properties. It is one of only two objects in the sample of about 300 objects with seven companions within 10 arcsec, and many of those companions themselves contribute to the 4, 5 and 6 companion bins. The overdensity of objects within 10 arcsec of 3C 254 is therefore a rare and significant occurrence in the I -band frame.

3 DISCUSSION

3.1 The photoionizing spectrum and the pressure of the gas surrounding 3C 254

FCFJ derived a pressure profile for the gas assuming that the ionizing spectrum of the quasar was described by a power law. The slope of this power law and its normalization was taken from Worrall et al. (1987). The energy index (α_v , where $f_v \propto \nu^{-\alpha_v}$) was 1.202. It was normalized to the rest-frame luminosity at 2500 \AA and the X-ray flux at 2 keV. In Section 2.1 it was shown that the optical and UV spectrum, down to a rest-frame wavelength of $\sim 850 \text{ \AA}$, is best fitted by a power law of energy index 0.7. The difference between this slope (and its normalization) and the one derived from Worrall et al. leads to a difference in the predicted ionizing flux from the quasar. If the slope derived above describes the spectrum up to an energy of R Rydberg,

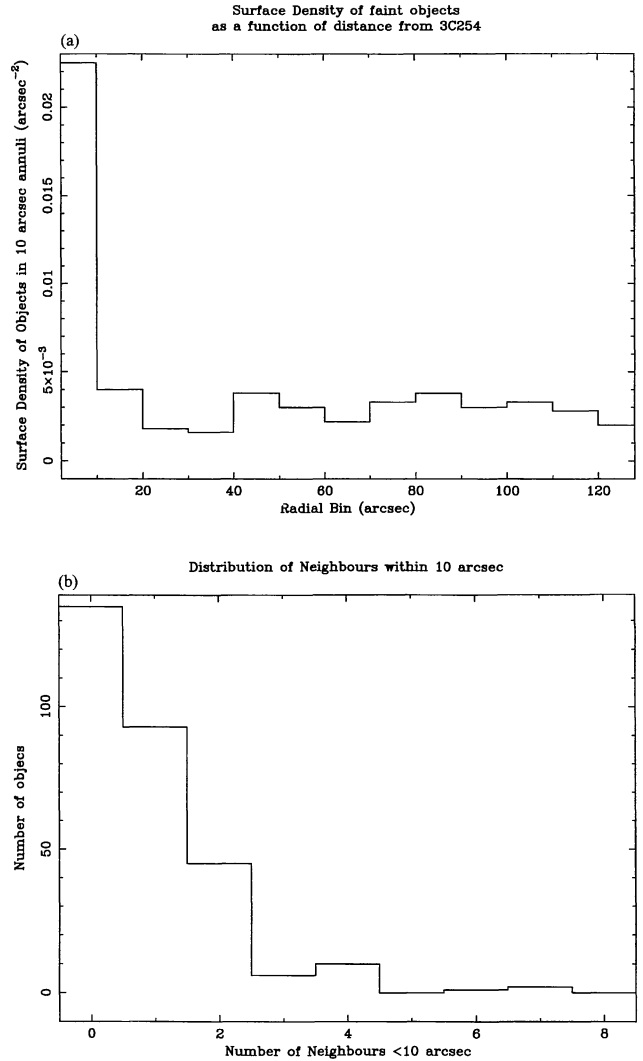


Figure 6. (a) Surface density of objects between 3 and 5 mag fainter in I than the quasar as a function of distance from the quasar. Objects are binned into 10 arcsec annuli. There is a clear excess of objects within 10 arcsec of 3C 254, implying that galaxies are clustered around 3C 254. (b) Histogram of the number of neighbouring faint objects within 10 arcsec of each of a sample of objects combining 3C 254 and the objects between 3 and 5 mag fainter than the quasar. Most objects have less than 3 faint companions. 3C 254 is one of two objects with seven faint companions, indicating that the overdensity shown in (a) is significant.

beyond which the spectrum turns over so that it fits the observed X-ray flux, then the Worrall slope under-predicts the ionizing photon flux by a factor of

$$f = 2.75^{-0.502} \times \frac{0.7(R^{-1.202} - 1)}{1.202(R^{-0.7} - 1)}.$$

For $R < 10$, the number of ionizing photons are underestimated by a factor of ~ 2 . This in turn means that the pressures derived by FCFJ were underestimated by a similar amount. This also increases the mass deposition rate of any inferred cooling flow around the quasar. The increase in pressure and mass deposition is similar to that found for 3C 263 by Crawford et al. (1991). In a similar way, the *IUE*

spectrum of this object showed that the estimate of the ionizing flux from 3C 263 derived from Worrall et al. was too low by a factor of ~ 5 .

3.2 The effect of the radio structure on the extended line emission

The spectroscopy of the [O II] and [O III] lines shows that part of the region of extended line emission around the eastern radio lobe is blueshifted relative to the nuclear emission lines. The close spatial association of this region with the eastern radio hotspot and lobe implies a real connection between these regions. A straightforward interpretation of this is that the emission line clouds are accelerated towards the observer by an interaction with the radio structure. The interaction strongly affects the propagation of the radio jet, leading to the large asymmetry in the radio structure. All of this implies that the eastern radio lobe is advancing towards the observer. Further south-eastwards, beyond the radio structure, the emission lines are approximately at rest relative to the nucleus. A similar velocity structure is seen in emission-line gas around the high redshift radio galaxy Tx1243+035 (van Ojik et al. 1996). In both this object and 3C 254 it seems clear that strong interactions between the radio structure and surrounding ionized gas results in induced bulk motion in the ionized gas. The path of the radio jet is strongly affected by these interactions.

At the point of interaction, the [O III]/[O II] line ratio is clearly increased in the blueshifted component relative to the more extended line emission. This is due in some way to the jet–gas interaction. One possibility is that the shocks driven into the gas by the interaction may have increased the ionization state of the gas, although shock models indicate that the lower (rather than higher) ionization lines can be enhanced in shocks (e.g. Sutherland, Bicknell & Dopita 1993; Koekemoer 1995). Another possibility is that the jet–gas interaction has shredded the (optically thick) gas clouds into many smaller clouds which are optically thin to Lyman continuum. This will increase the surface brightness of the line emission in this region and increase the [O III]/[O II] ratio, as the [O II] is only strongly produced in optically thick photoionized clouds (Bremer, Fabian & Crawford 1996).

The region of jet–cloud interaction is localized to the 1–2 arcsec east of the nucleus. The emissions beyond the eastern hotspot in the spectra presented here are unaffected by the propagation of the radio source, as the radio jet has never entered that region. Similarly, the spectra in FCFJ are taken at three different position angles around the source, and the overall ionization state of the gas does not seem to depend on the position relative to the radio structure, but mainly on the distance from the nucleus (much of the emission extends considerably beyond the radio structure). Clearly, in those cases where there is evidence for a considerable interaction between the optical emission-line gas and the radio structure, the ionization state of the gas can be a poor tracer of the surrounding environment (as it is for the high-ionization blueshifted system in 3C 254). In the case of 3C 254, the pressure estimates in FCFJ are largely unaffected by the jet–gas interaction, as most of the extended emission-line gas is beyond the bounds of the radio source.

3.3 The cluster around 3C 254

One implication of the high pressure deduced by FCFJ for the nebulosity surrounding 3C 254 was that the object should be in a cluster. The images of 3C 254 show clear evidence for a surrounding group or cluster. The magnitudes and colours of the surrounding objects are comparable to those of models for passively evolving L^* ellipticals at $z=0.734$ (e.g. Guiderdoni & Rocca-Volmerange 1988; Bruzual & Charlot 1993) with a redshift of formation $z_f > 2$.

The distribution of objects around the quasar makes the classification of the cluster or group difficult as most classifications are based on the density of objects over a much larger radius. It is notable that the studies of clustering of galaxies around distant quasars (e.g. Hutchings 1995; Hutchings, Crampton & Johnson 1995) also show overdensities of objects close to the quasars which look far more compact than would be expected if the objects were in a high redshift analogue of a rich Abell cluster.

It is possible that the objects surrounding the quasar are in a foreground cluster not associated with the quasar. The coincidence of the cluster and quasar could be attributed to gravitational lensing of the quasar by the cluster. However, the present optical and radio data show no evidence for lensing. The quasar core is very weak relative to the hotspots, so it is unlikely the nucleus is lensed. The extended radio and optical structures also show none of the usual signs of gravitational amplification or distortion.

The objects close to the quasar seem to be distributed very roughly along a line in the direction of the current radio axis and extended optical emission (e.g. see Fig. 5d). There are other objects within 1 arcmin with similar brightness to the companion objects which also roughly lie on a line cutting through the quasar at a similar position angle to the line between the nucleus and the nearest radio lobe. This may be a random effect, but if real could be to do with the merger history of the cluster around the quasar (West 1994) or could be explained by objects photoionized by a narrow (BL Lac-like) beam from the quasar. A similar statistical effect has been noted by Röttgering et al. (1995) in a sample of RGs.

3.4 Extended emission, unification schemes and the alignment effect

The extended line and continuum emission seen in 3C 254 is very similar in nature to the emission from RGs (e.g. see McCarthy, Spinrad & van Breugel 1995). Whereas there are many examples in the literature of ‘aligned’ RGs, there have been only a few attempts to image the fuzz around RLQs at high enough redshift to expect to detect both aligned continuum and line emission based on experience of the RGs (e.g. Heckman et al. 1991; Hutchings 1992). The images of 3C 254 presented here show aligned, extended continuum and line emission more clearly than any of these studies. It is notable that the clearly aligned continuum is found in a RLQ with $z > 0.7$ as the continuum alignment effect in RGs is generally only detected above this redshift.

This supports the idea that RLQs and RGs are found in the same kind of environment. This is a prerequisite for orientation dependent unification schemes, where RGs and

quasars differ in their observed properties as they are viewed at different angles to the line of sight (Scheuer 1987; Barthel 1989). In these schemes, the radio axes of RGs lie close to the plane of the sky, the radio axes of the quasars lie closer to the line of sight to the object. The greater the radio core dominance, the closer the radio axis is to the line of sight, the core emission enhanced by doppler boosting.

There are reasons to believe that the emission axis of 3C 254 is closer to the plane of the sky than for most other 3C quasars. It has a large (80 kpc) extended emission-line region in comparison to other RLQs studied by Bremer et al. (1992), FCFJ, etc. It has a very weak radio core compared with other 3C quasars (e.g. Jackson & Browne 1991a,b; Hooimeyer et al. 1992). Although 3C 254 has an angular size in the radio typical for a 3C quasar and smaller than an average 3C galaxy, this is at least in part due to the small distance between the nucleus and eastern hotspot. Taking its ‘true’ size to be double the nucleus–western hotspot distance would make the angular size of 3C 254 comparable to that of any average 3C galaxy.

3C 254 could be an important ‘crossover’ object between RGs and RLQs in terms of these schemes. This may be because it is viewed just at the maximum angle to the radio axis for it to be seen as a quasar (about 45° in the simplest unification scheme), or because it is viewed at a larger angle and has a broader ionization cone than most quasars. These observations also provide evidence for any unification scheme where RGs and RLQs exist in similar environments and for any scheme where lobe dominated quasars are strongly related to radio galaxies.

Most [O II] emission from 3C 254 arises in the extended emission-line region, whereas the [O III] is dominated by strong nuclear emission. The [O II] luminosities of 3C quasars in general (Hes, Barthel & Fosbury 1993; Bremer et al. 1992) are similar to those of 3C radio galaxies, where [O III] emission is stronger in quasars (Jackson & Browne 1990). The difference in behaviour of these two lines can be understood if, in quasars, we see a region of line emission close to the nucleus that is not seen in the galaxies (because of an obscuring torus, for example). If the density of line-emitting gas in this region is above the critical density for [O II], but not for [O III], then only [O III] will be seen in this region.

Several theories which attempt to explain the continuum alignment effect have been proposed. The main theories are jet-induced star formation (e.g. Rees 1989; Chambers & Miley 1989), scattering of nuclear light into our line of sight (either by dust, e.g. Tadhunter, Fosbury & di Serego Alighieri 1988, or hot electrons, Fabian 1989), and nebular continuum emitted by the emission-line clouds (Dickson et al. 1995). Detection of polarized emission from radio galaxies (e.g. Tadhunter et al. 1992; di Serego Alighieri, Cimatti & Fosbury 1994) implies that at least some of the continuum is scattered radiation. Unlike in radio galaxies, the nucleus of 3C 254 is visible, allowing a direct comparison of the colours of the extended continuum with those of the nucleus. Unfortunately, although large-scale fuzz is redder by about 0.5 mag in $U-R$ than the nucleus of 3C 254, the uncertainties (e.g. line contamination) in this measurement mean that they cannot be used to rule in or out any of the above origins for the fuzz. To do that, line-free *HST* images, or spectropolarimetry are required. What is clear is that the fuzz is about as blue as the aligned light in many RGs.

3.5 Correlations between the optical and the radio structure of 3C 254

Several correlations between the optical and radio structures of powerful RGs and RLQs have been discovered. McCarthy et al. (1991) carried out a study of the relationship between the radio structure and the extended emission-line regions in powerful 3C RGs. In almost all objects the radio lobe closest to the nucleus of a radio galaxy was on the same side of the nucleus as the highest surface brightness extended optical line emission. This implies a direct environmental link between extended emission-line regions and the radio structure of RGs. Also included in the sample were several RLQs, although no optical data were presented for these objects. 3C 254 was included in this sub-sample. Notably, this was the object with the most asymmetric radio structure of all the RGs and RLQs. Typically, the ratio of the distances of the two radio hotspots to the nucleus is $\sim 1-2$ whereas for 3C 254 it is 6.8. These observations show that 3C 254 also obeys the correlation found by McCarthy, van Breugel & Kapahi.

The eastern radio lobe of 3C 254 is the most depolarized (Liu & Pooley 1991). This is expected given the results of FCFJ. The eastern radio lobe is closer to the nucleus, and therefore closer to the centre of a surrounding hot halo than the western lobe. FCFJ showed that the pressure and density of a surrounding halo continued to increase close to the nucleus of 3C 254. The depolarizing effect of a Faraday screen is a function of the magnetic field strength, the path length through the screen and the electron density in the screen. The difference in the electron densities around the two lobes can explain the difference in the polarization between them. The blueshifted emission lines on the eastern side imply that the most depolarized lobe is coming towards the observer.

This is in contradiction to the Garrington–Laing effect (Garrington et al. 1988; Laing 1988), where the radio emission on the (approaching) jet side is less depolarized than that on the counter-jet side in quasars with one-sided radio jets. The explanation for this is that it is a projection effect. The jet side is seen through a shorter path length of a surrounding hot halo (the hot ICM of a surrounding cluster) than the counter-jet side and consequently suffers less depolarization (Garrington & Conway 1991). The polarization structure of 3C 254 can be reconciled with this explanation if the difference in the density of the hot phase surrounding the east and west radio lobes outweighs any path length difference. This again requires that the radio axis of 3C 254 is relatively far from the line of sight in comparison to other quasars.

Liu & Pooley (1991) showed that the most depolarized of the two radio lobes in RGs and lobe-dominated quasars also had the steeper radio spectrum. 3C 254 obeys this correlation, pointing to an environmental origin for polarization variations in these sources. This can only be reconciled with the Garrington–Laing effect and orientation-based unification schemes in Faraday depolarization introduced by side-to-side path-length differences in quasars with single sided jets are of the same order, or slightly more than those introduced by side-to-side environmental differences. If environmental effects dominate then we should never see the Garrington–Laing effect. If path-length effects domi-

nate, they should swamp environmental differences, even in sources with radio axes moderately close to the plane of the sky, and the Liu & Pooley correction would not be observed.

3.6 Extended emission and cooling flows

The original motivation for the study of 3C 254 by FCFJ was to determine whether this quasar (amongst others) was surrounded by emission-line nebulosity signifying that the quasar was in a cluster containing a cooling flow. The $[\text{O III}]/[\text{O II}]$ line ratio in the extended emission and the photoionizing luminosity of the quasar indicated that the line-emitting gas was at high pressure ($> 10^6 \text{ cm}^{-3} \text{ K}$ within 30 kpc of the nucleus). Section 3.1 shows that the pressure and therefore the mass deposition rate around the quasar may be even higher, given a more detailed model of the ionizing spectrum.

The most obvious prediction of the previous work is that 3C 254 should be in a group or cluster of galaxies, and therefore be surrounded by an overdensity of faint objects in comparison to the field. The results of Section 2.3.2 confirm this prediction. The polarization structure of the radio emission from 3C 254 is also consistent with the results of FCFJ, as shown in the previous section.

The high pressure of the gas surrounding 3C 254 (FCFJ) implies a high cooling and mass deposition rate for the hot phase surrounding 3C 254. Even if only a small fraction of the cooling material formed stars, the host galaxy should be blue, showing signs of recent or ongoing star formation. The colour of the fuzz around 3C 254 is blue, but from these results it is impossible to tell how much emission comes from stars.

The velocity structure of the emission-line gas is not predicted by the cooling flow scenario. However, it is likely that part of the velocity structure is due to an interaction between the emission-line gas and the radio structure of the quasar. This is compatible with the cooling flow scenario (see Bremer, Fabian & Crawford 1996), indeed many cooling flows in low redshift clusters have optical emission lines with velocity widths that can only be explained by some form of turbulence acting on the emission-line clouds.

4 CONCLUSIONS

3C 254 is in a group or cluster of galaxies, as required by the explanation of the origin of the extended $[\text{O II}]$ and $[\text{O III}]$ emission given by FCFJ. The pressure of the ICM around 3C 254 is probably twice the value determined in that work, given the UV spectrum of the quasar.

The extended line emission previously detected by FCFJ is aligned with the radio axis of the quasar. The optical continuum is similarly aligned. This is the best case of a RLQ with aligned extended continuum and it occurs in one of the most lobe dominated 3C quasars. This has important implications for unification schemes. The extended structure of 3C 254 is very similar to the extended emission found around similar redshift RGs, in strong agreement with the predictions of unification schemes based on line-of-sight effects such as those of Barthel (1989) and Scheuer (1987). In these schemes, the most lobe dominated quasars will

have extended optical properties most like those of radio galaxies.

The extended continuum emission is blue, consistent with those of the extended continuum of RGs at similar redshifts. Further observations are required to determine the nature of the extended continuum. As the nucleus of 3C 254 is visible a clear comparison of nuclear and off-nuclear colours will be possible (unlike in the case of radio galaxies).

Part of the extended line emission arises from a region undergoing an interaction with the eastern radio lobe. The emission lines at that point are blueshifted by $\sim 650 \text{ km s}^{-1}$ relative to the nucleus, and have a higher ionization state relative to the rest of the extended emission-line region. The rest of the extended emission lines in these spectra, and in those of FCFJ are not in regions interacting with the radio source. Consequently, the pressure estimates of FCFJ are not confused by the effects of jet-cloud interactions.

Most of the narrow $[\text{O II}]$ emission arises from the extended line emission, not the classical narrow-line region (unlike the $[\text{O III}]$ emission). As the emission axis of the quasar is closer to the plane of the sky than for most other quasars, this may occur in many RLQs, but would be less obvious due to foreshortening of the extended emission. This finding is consistent with previous results showing that the $[\text{O II}]$ fluxes in radio galaxies and radio loud quasars of similar radio luminosities are comparable (e.g. Hes et al. 1993; Bremer et al. 1992), whereas the $[\text{O III}]$ fluxes of the two classes are different (e.g. Jackson et al. 1991a,b).

The correlations noted by other authors between the radio and optical properties of RGs are also found in 3C 254. The brightest extended line emission is on the side of the closest radio lobe. The radio hotspot with the steepest spectrum is the most depolarized and on the most luminous side of the radio structure and the closest to the nucleus.

A key test of orientation dependent unification schemes is the similarity (or otherwise) of the extended optical emission of RLQs and RGs. 3C 254 could prove to be an extremely useful source in investigating the similarities and differences in the immediate environments of powerful RGs and RLQs, as the observed optical and radio properties of this quasar are dominated by environmental effects, rather than orientation and projection effects. If 3C 254 turns out to be a typical lobe-dominated RLQ in terms of its extended optical and IR properties then the case of unification schemes such as that of Barthel (1989) will be strengthened. In these schemes the lobe-dominated quasars should have extended optical and IR properties similar to radio galaxies. If it is found that the extended optical and IR properties of radio-loud quasars do not correlate with the relative strengths of lobe and core emission, then the same unification schemes will be in severe difficulty. It should be noted that as with many similar observations, distinguishing between orientation dependent schemes and others which also require RLQs and RGs to be in similar environments will be difficult.

ACKNOWLEDGMENTS

The WHT is operated by the Royal Greenwich Observatory at the Spanish Observatorio de Astrofísica de Canarias. UKIRT is operated by the Royal Observatory Edinburgh on behalf of the PPARC. David Schade is thanked for obtain-

ing the CFHT image. Carolin Crawford is thanked for much help during the initial stages of this work. MNB acknowledges financial support from the EC twinning project, a programme subsidy granted by the Netherlands Organization for Scientific Research (NWO).

REFERENCES

- Barthel P. D., 1989, *ApJ*, 336, 606
 Bremer M. N., Crawford C. S., Fabian A. C., Johnstone R. M., 1992, *MNRAS*, 254, 654
 Bremer M. N., Fabian A. C., Crawford C. S., 1996, *MNRAS*, in press
 Bruzual G., Charlot S., 1993, *ApJ*, 405, 538
 Chambers K. C., Miley G. K., 1989, in Kron R. G., ed., *ASP Conf. Proc.*, Vol. 10, *The Evolution of the Universe of Galaxies, The Edwin Hubble Centennial Symposium*. Astron. Soc. Pac., San Francisco, p. 373
 Christian C. A., Adams M., Barnes J. V., Butcher H., Hayes D. S., Mould J. R., Siegel M., 1985, *PASP*, 97, 363
 Crawford C. S., Fabian A. C., 1989, *MNRAS*, 239, 219
 Crawford C. S., Fabian A. C., Johnstone R. M., 1988, *MNRAS*, 235, 183
 Crawford C. S., Fabian A. C., George I. M., Naylor T., 1991, *MNRAS*, 248, 139
 Dickson R., Tadhunter C., Shaw M., Clark N., Morganti R., 1995, *MNRAS*, 273, 29
 di Serego Alighieri S., Cimatti A., Fosbury R. A. E., 1994, *ApJ*, 431, 123
 Fabian A. C., 1989, *MNRAS*, 238, 41P
 Fanaroff B. L., Riley J. M., 1974, *MNRAS*, 167, 31P
 Forbes D. A., Crawford C. S., Fabian A. C., Johnstone R. M., 1990, *MNRAS*, 244, 680 (FCFJ)
 Garrington S. T., Leahy J. P., Conway R. G., Laing R. A., 1988, *Nat*, 331, 14
 Garrington S. T., Conway R. G., 1991, *MNRAS*, 250, 198
 Guiderdoni B., Rocca-Volmerange B., 1988, *A&AS*, 74, 185
 Heckman T. M., Lehnert M. D., van Breugel W., Miley G. K., 1991, *ApJ*, 370, 78
 Hes R., Barthel P. D., Fosbury R. A. E., 1993, *Nat*, 362, 326
 Hooimeyer J. R. A., Barthel P. D., Schilizzi R. T., Miley G. K., 1992, *A&A*, 261, 18
 Hutchings J. B., 1992, *AJ*, 104, 1311
 Hutchings J. B., 1995, *AJ*, 109, 928
 Hutchings J. B., Crampton D., Johnson A., 1995, *AJ*, 109, 73
 Jackson N., Browne I. W. A., 1990, *Nat*, 343, 43
 Jackson N., Browne I. W. A., 1991a, *MNRAS*, 250, 414
 Jackson N., Browne I. W. A., 1991b, *MNRAS*, 250, 422
 Koekemoer A. M., 1995, PhD thesis, Australian National Univ.
 Laing R. A., 1988, *Nat*, 331, 149
 Landolt A., 1983, *AJ*, 88, 439
 Liu R., Pooley G., 1991, *MNRAS*, 249, 343
 McCarthy P. J., 1993, *ARA&A*, 31, 639
 McCarthy P. J., van Breugel W., Kapahi V., 1991, *ApJ*, 371, 478
 McCarthy P. J., Spinrad H., van Breugel W., 1995, *ApJS*, 99, 27
 Owen F. N., Puschell J. J., 1984, *AJ*, 89, 932
 Rees M. J., 1989, *MNRAS*, 239, 1P
 Röttgering H. J. A., West M. J., Miley G. K., Chambers K. C., 1996, *A&A*, 307, 376
 Scheuer P. A. G., 1987, in Zensus A., Pearson T. J., eds, *Superluminous Radio Sources*. Cambridge Univ. Press, Cambridge, p. 104
 Sutherland R. S., Bicknell G. V., Dopita M. G., 1993, *ApJ*, 414, 510
 Tadhunter C., Fosbury R. A. E., di Serego Alighieri S., 1988, in Maraschi L., Maccacaro T., Ulrich M. H., eds, *Proc. The Como Conference, BILac Objects*. Springer Verlag, Berlin, p. 79
 Tadhunter C., Scarrott S. M., Draper P., Rolph C., 1992, *MNRAS*, 256, 53P
 van Ojik R., Röttgering H. J. A., Carilli C., Bremer M. N., Miley G. K., 1996, *A&A*, 313, 25
 West M. J., 1994, *MNRAS*, 286, 79
 Wills B. J., Netzer H., Brotherton B. S., Han M., Wills D., Baldwin J. A., Ferland G. J., Browne I. W. A., 1993, *ApJ*, 410, 534
 Worrall D. M., Giommi P., Tananbaum H., Zamorani G., 1987, *ApJ*, 313, 596